Surface & Coatings Technology 281 (2015) 150–156

Contents lists available at ScienceDirect

Surface & Coatings Technology

journal homepage: www.elsevier.com/locate/surfcoat

Industrial-scale high power impulse magnetron sputtering of yttria-stabilized zirconia on porous NiO/YSZ fuel cell anodes

Steffen Sønderby [a,b], Bjarke H. Christensen [b], Klaus P. Almtoft [b], Lars P. Nielsen [b], Per Eklund [a,*]

[a] Thin Film Division, Department of Physics, Chemistry and Biology, IFM, Linköping University, SE-58183 Linköping, Sweden
[b] Danish Technological Institute, Tribology Centre, Teknologiparken, Kongsvang Allé 29, DK-8000 Aarhus C, Denmark

ARTICLE INFO

Article history:
Received 15 June 2015
Revised 29 September 2015
Accepted in revised form 30 September 2015
Available online 3 October 2015

Keywords:
Physical vapor deposition (PVD)
Solid oxide fuel cell (SOFC)
YSZ
HPPMS

ABSTRACT

Yttria-stabilized zirconia (YSZ) thin films are reactively sputter-deposited by high power impulse magnetron sputtering (HiPIMS) in an industrial setup on porous NiO/YSZ fuel cell anodes. The influence of deposition pressure, cathode peak power density, and substrate bias voltage on the deposition rate and film morphology is studied. It is seen that increasing the deposition pressure from ~370 mPa to ~750 mPa results in a 64% increase in the deposition rate and denser film. Films are deposited at peak power densities ranging from 0.4 kW cm^{-2} to 1.1 kW cm^{-2}. By increasing the peak power density the degree of ionization of both Ar and sputtered metallic species is significantly increased which results in denser films as open column boundaries are removed. The increase in peak power also results in a considerable drop in deposition rate. By combining a peak power density of 0.6 kW cm^{-2} with the application of −180 V substrate bias voltage a homogenous and essentially column-free coating can be deposited. These results demonstrate HiPIMS deposition as being capable of producing dense YSZ coatings on porous substrates as needed for solid oxide fuel cell applications.

1. Introduction

Yttria-stabilized zirconia (YSZ) has been extensively studied and is often the material of choice for solid oxide fuel cell (SOFC) electrolytes. This is because YSZ has an acceptable ionic conductivity, is electrically insulating, chemically inert and relatively cheap to process compared to other possible electrolyte materials. As the ionic conductivity is highly dependent on temperature, SOFCs are often operated around 800–1000 °C in order to reach a sufficient efficiency. These high temperatures result in increased reactivity of the cell core components and the use of expensive interconnect materials [1]. Therefore, it is of interest to reduce the operation temperature. Another benefit of reduced operation temperatures is the possibility to introduce the metal-supported SOFC as an alternative to the ceramic-supported cell. The metal-supported SOFC design has several advantages compared to ceramic-supported cells. These include low material costs and high robustness of the metallic substrate, which is advantageous both in the production line and in applications such as auxiliary power units [2].

One way of lowering the SOFC operation temperature to an intermediate temperature domain of 500–700 °C is by developing thin film electrolytes and thereby minimizing the ohmic losses in the electrolyte [1,3,4]. YSZ electrolytes have typically been fabricated by tape-casting, screen-printing, or spraying techniques followed by subsequent sintering [5]. These techniques are ideal for producing at low cost with high throughput but are not suitable for producing dense and thin (a few μm in thickness) YSZ electrolytes. Several groups have demonstrated the synthesis of thin YSZ films employing a variety of chemical and physical deposition methods [3] such as chemical vapor deposition (CVD) [6], atomic layer deposition (ALD) [7], spin coating [8], pulsed laser deposition (PLD) [9,10] and magnetron sputtering [11–16].

Magnetron sputtering is a promising technique for the industrial-scale production of YSZ thin films [15]. However, because of the high melting temperature of YSZ (~2700 °C [17]) it is difficult to achieve the adatom mobility of the deposited species necessary to obtain dense coatings without applying high deposition temperatures [16]. For industrial deposition of YSZ, the increased cycle time due to heating and subsequent cooling is problematic as it reduces throughput. Another potential problem is connected to reactive thin film deposition on metal-supported cells as the combination of elevated temperatures and oxygen present for the reactive deposition process may result in the formation of nonconductive oxide phases in the metal-support which will decrease cell performance. However, for films deposited below 400 °C we have shown that the metal-support is not damaged [18].

High power impulse magnetron sputtering (HiPIMS) is a PVD technique, which is characterized by a highly ionized deposition flux. This is achieved by applying to the sputtering target short high power

* Corresponding author.
E-mail address: perek@ifm.liu.se (P. Eklund).

http://dx.doi.org/10.1016/j.surfcoat.2015.09.058

density pulses with a duty cycle of a few percent [19–20,21]. As a result, plasmas with electron densities several orders of magnitude higher than those in conventional magnetron sputtering techniques, such as direct current magnetron sputtering (DCMS), are generated [22]. The formed plasma causes ionization of a large fraction of sputtered atoms [22,23]. By applying a substrate, bias voltage the ionized deposition flux can be steered to the substrate and cause an intense energetic bombardment of the growing film. DCMS deposition of YSZ electrolytes often results in a columnar microstructure, which may cause internal leakage in the cell leading to a decreased open cell potential [24,25]. It has been shown that the high-flux ion irradiation characteristic of HiPIMS can be used to suppress the columnar and underdense microstructure typically seen in films deposited at low substrate temperatures [21,26]. Therefore, HiPIMS may be a suitable technique for YSZ deposition for SOFC applications [27].

In this study, industrial-scale HiPIMS deposition of YSZ is investigated. The influence of deposition pressure, cathode peak power density, and substrate bias voltage on the deposition rate and film morphology is studied.

2. Experimental details

The films were deposited by reactive HiPIMS, and pulsed DCMS for reference, in a commercial batch-coating system (CC800/9, CemeCon AG) on 13 × 13 cm^2 porous NiO–YSZ fuel cell anodes and 1.5 × 1.5 cm^2 Si(001). The substrates were mounted on a substrate table carrying out a one-fold rotation. Because of the rotation, the substrates were only facing the sputtering targets part of the time. When the targets were directly facing the substrates the target–substrate distance was 6.5 cm.

Two targets (50 × 8.8 cm^2) were positioned on each side of the mounting stage, facing each other. The targets were metallic Zr–Y (86:14 at.%) of 99.5% purity and were sputtered in an Ar/O_2 atmosphere (purity 99.999%). The Ar gas flow was 600 sccm and the oxygen flow was 45–75 sccm. The working pressure was varied between depositions from 370–750 mPa. Since deposition in metallic mode results in substoichiometric films and the coating unit did not have a built-in feedback mechanism to maintain deposition in the transition region, which is inherently unstable [28], all films were deposited in poisoned mode. Before deposition at a certain set of parameter, the hysteresis effect was measured to find the oxygen flow that would ensure deposition in poisoned mode. For all HiPIMS conditions reported on in this paper, the transition from metallic to poisoned mode was found by observing an increase in peak current of more than 200 A. The oxygen flow needed to poison the target was dependent on the depth of racetrack and decreased when the target was worn. Therefore, the oxygen flow was tuned between depositions in order to secure that all depositions were carried out at approximately the same position on the hysteresis curve.

Prior to depositions, the chamber was evacuated to a base pressure below 1 mPa and the samples were pre-heated to ~350 °C but no heating was applied during deposition. The pre-heating was carried out to prevent outgassing during deposition where temperatures up to ~300 °C could be reached due to the energetic bombardment by ions, electrons and fast neutral species. After pre-heating, the chamber was cooled for 20 min to make sure that the temperature was below 300 °C before starting the deposition. Deposition temperatures were measured by a thermocouple placed at the position of the substrate table.

The targets were operated in unipolar mode using a pulse width of 100 μs and an average power of 5 kW. The repetition frequency was varied in order to vary the pulse peak power. A unipolar pulsed DC bias voltage with a frequency and on-time equal to the HiPIMS repetition frequency was applied to the substrate table and synchronized with the HiPIMS discharge. Bias voltages ranging from floating potential (no bias) to −180 V were used in different depositions. During the processes, the voltage and current waveforms of the targets, as well as the substrate table, were recorded with an oscilloscope (Tektronix DPO 2024). Examples of the waveforms recorded for HiPIMS discharges with power densities of 1.1 kW cm^{-2} and 0.4 kW cm^{-2} are seen in Fig. 1. Due to variations in growth rate because of the varied deposition parameters, the deposition time was adjusted in order to achieve film thicknesses in the range 2.5–3 μm. For comparison, reference samples were deposited by pulsed DCMS at 5 kW average power in poisoned mode. The two pulsed DCMS cathodes were placed next to each other in the same side of the coating unit and were operated in dual pulsed mode with a frequency of 50 kHz and a duty cycle of 50%. A substrate bias voltage with a frequency of 250 kHz and a reverse time of 1 μs was applied to the substrates.

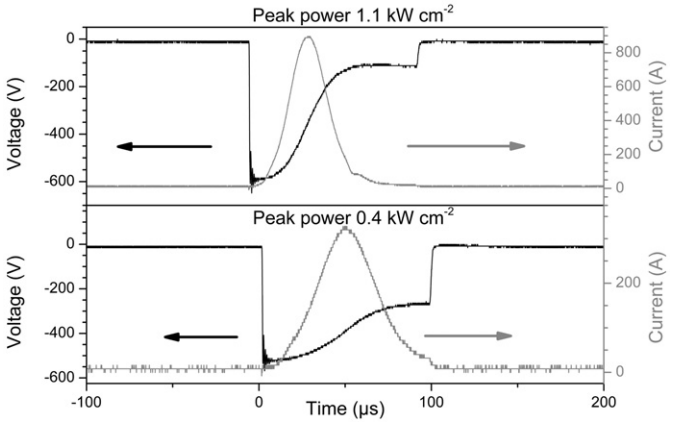

Fig. 1. Examples of waveforms from HiPIMS discharges with power densities of 1.1 kW cm^{-2} and 0.4 kW cm^{-2}.

Measurements by optical emission spectroscopy (OES, from Avantes BV) were acquired for qualitative analysis of ion and excited neutral densities in the plasma at different peak powers. The spectra were collected in the wavelength range 250–770 nm with the spectrometer lens positioned parallel to the target surface at a distance of 2 cm. Scanning electron microscopy (SEM, Nova 600 nanoSEM from FEI) was used to determine the film morphology as well as film thickness. X-ray diffraction (XRD) measurements in the θ–2θ geometry were performed with a Bruker D8 Discover diffractometer on samples deposited on Si(001) using CuK_α radiation. The purpose of XRD was primarily to confirm that cubic YSZ was obtained, as the growth on Si(001) is significantly different from that on the porous NiO–YSZ fuel cell anodes [15].

3. Results and discussion

In order to study the influence of deposition pressure, cathode peak power density, and substrate bias voltage on the deposition rate and film morphology three series of depositions were carried out. To study the effects of working pressure films were deposited at ~370 mPa and ~750 mPa. The peak power density was 0.9 kW cm^{-2} and no bias voltage was applied. It was not deemed applicable to increase the working pressure further as high working pressures result in ionic species being thermalized before reaching the substrate [29]. The effects of the peak power density were studied by carrying out depositions with peak power densities varying from 0.4–1.1 kW cm^{-2}. Films were deposited at a pressure of ~750 mPa and a substrate bias voltage of −60 V was applied. In the last series of depositions the influence of substrate bias voltage was investigated. Depositions were carried out at substrate bias voltages of −60 V, −120 V, and −180 V. The peak power density was set to 0.6 kW cm^{-2} and the pressure to ~750 mPa.

To confirm the crystallographic phase of the deposited films XRD was performed on samples deposited on Si(001). All films were found to possess the cubic structure. Two selected X-ray diffractograms are shown in Fig. 2. The films are seen to be compressively stressed as the

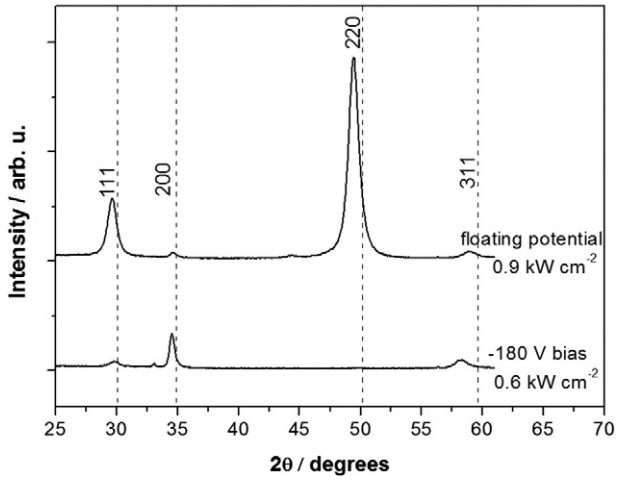

Fig. 2. θ–2θ X-ray diffractograms of selected YSZ films deposited on Si(001) at ~750 mPa. Dashed lines mark peak positions in the powder diffractogram (ICDD JCP2 No. 30-1468).

peaks are shifted to lower angles compared to the powder diffractogram reference (ICDD JCP2 No. 30-1468). The shown X-ray diffractograms represent two different textures observed in the deposited films depending on how energetic the ion bombardment was during film growth. The film deposited at a peak power density of 0.9 kW cm^{-2} and floating potential is seen to be <220> textured whereas the films deposited at 0.6 kW cm^{-2} and −180 V substrate bias is <200> textured. Dissociation of molecular O_2 is likely to occur, and to be a more dominant effect compared to dc magnetron sputtering due to the relatively high electron energies and densities under HiPIMS conditions. Mahieu et al. [30] have shown [220] to be the fastest growing direction for YSZ when the reactive gas is atomic oxygen. Therefore, the <220> texture can be explained by competitive growth. The films deposited under the influence of a substrate bias are bombarded by high energetic Ar- and metal-ions. In Fig. 2, the film deposited at a bias voltage of −180 V is seen to be <200> textured, which can be explained as a result of channeling [11]. It should be noted that when depositing YSZ on porous YSZ substrates a template effect is to be expected resulting in the film to be growing with the same orientation as the underlying YSZ substrate [15].

3.1. Deposition pressure effects

Similar to conventional magnetron sputtering, the working pressure is an important parameter during HiPIMS deposition as it influences the deposition rate and determines the mean free path of the sputtered species which in turn affects the energy of species arriving at the substrate [31]. The working pressure therefore influences both deposition rate and film density [31]. Therefore, it is important to determine a working pressure, which will allow for deposition of void-free films at a reasonable deposition rate. Films were deposited at working pressures of ~370 mPa and ~750 mPa for comparison. Table 1 shows deposition parameters for the deposited films (determined from SEM cross sections, not corrected for film-density effects, which are treated separately). By increasing the working pressure the deposition rate is increased from 0.14 μm h^{-1} to 0.23 μm h^{-1}, a 64% increase. The lower deposition rate at a working pressure of ~370 mPa may be a result of the high peak current (see Table 1) as it is known that increasing the peak current density may result in decreased deposition rates due to self-sputtering [26]. In addition, the increased peak power is likely to result in increased ionization of the sputtered material close to the target surface. Many ionized particles will be attracted back to target surface and thus be lost for the deposition.

Fig. 3 shows SEM micrographs of the NiO–YSZ substrate surface as well as film surfaces. The substrate is seen (from the contrast between grains) to consist of sintered NiO and YSZ grains and have several approximately 0.5–1 μm large pores (black areas in Fig. 3.a). The deposited films reproduce the morphology of the underlying substrate. The film deposited at ~370 mPa (Fig. 3.b) has a very open structure and several voids are seen. The film deposited at ~750 mPa appears denser but a few voids can be observed (Fig. 3.c). It is likely that the increased flux of bombarding ionic species at higher pressure increases adatom mobility (note that any decrease in adatom energy due to increased scattering will still be rather modest at this deposition pressure) and thus reduces the concentration of intercolumnar voids in the film deposited at ~750 mPa [32]. This explanation is further verified by the deposition temperature increasing from ~220 °C to ~280 °C. The temperature increase is solely due to bombardment of plasma species as no substrate heating is applied.

3.2. Influence of peak power

To improve the film density the effect of the HiPIMS peak power density was investigated. Films were deposited at a pressure of ~750 mPa as pressures in this range were seen to result in fewer intercolumnar voids. A substrate bias voltage of −60 V was applied. For comparison a film was deposited by pulsed DCMS.

Emission spectra of the plasma at different peak power densities were recorded. As it was not possible to place the lens at the position of the substrate as it would be hit by the rotating mounting platform the spectra were recorded closer to the target. Thus, the measured data does not exactly describe the situation at the substrate but gives indication of which species may reach the growing film. In order to compare the degree of ionization under different conditions peaks for neutral and ionic Ar (Ar^0: 763.5 nm, Ar^+: 480.6 nm) and Zr (Zr^0: 468.7 nm, Zr^+: 256.8 nm, Zr^{2+}: 262.0 nm) were chosen and the intensity ratio of ionic to neutral species was plotted in Fig. 4. As can be seen in the figure, HiPIMS plasma has a significantly higher degree of ionization than pulsed DCMS and the degree of ionization of both Ar and Zr increases as the peak power density is increased. Above 0.5 kW cm^{-2}, the doubly ionized Zr^{2+} increases more rapidly than Zr^+.

Fig. 5 shows SEM cross-sections of HiPIMS films deposited at cathode peak power densities of 0.4 kW cm^{-2}, 0.6 kW cm^{-2}, and 1.1 kW cm^{-2}, as well as a pulsed DCMS film (Fig. 5.d) for comparison. The film deposited at 0.4 kW cm^{-2} (Fig. 5.a) is columnar with visible

Table 1
Deposition pressures, oxygen flow, peak power densities, peak current, peak voltage, repetition frequency, substrate bias voltages, and deposition rates during depositions.

	Pressure variation		Peak power density variation				Substrate bias variation		Pulsed DCMS
Pressure (mPa)	370	750	750	750	750	750	750	750	750
Oxygen flow (sccm)	75	70	55	55	50	45	70	70	50
Peak power density (kW cm^{-2})	0.9	0.9	0.4	0.6	0.7	1.1	0.6	0.6	–
Peak current (I)	840	700	315	500	611	885	470	546	–
Peak voltage (V)	510	568	510	528	530	576	596	603	–
Repetition frequency (kHz)	0.8	0.8	1	0.8	0.7	0.6	0.8	0.8	–
Substrate bias (V)	Floating potential	Floating potential	60	60	60	60	120	180	60
Deposition rate (μm h^{-1})	0.14	0.23	0.78	0.42	0.37	0.20	0.30	0.21	1.2

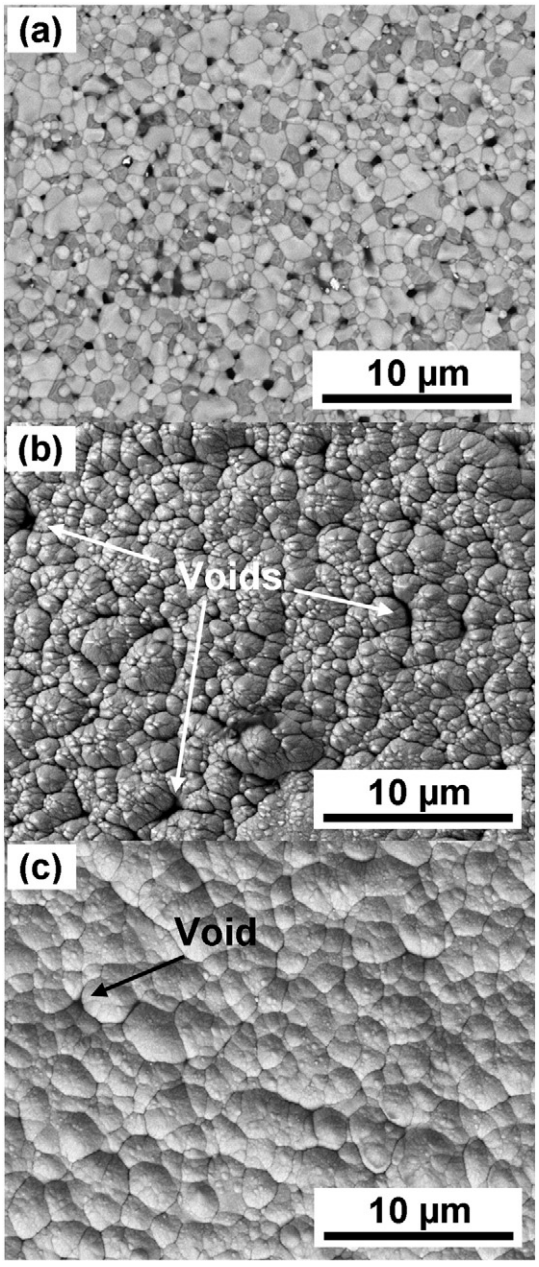

Fig. 3. SEM micrographs of (a) the porous NiO/YSZ substrate, YSZ films grown at floating potential, a peak power density of 0.9 kW cm^{-2} and a working pressure of (b) ~370 mPa and (c) ~750 mPa.

intercolumnar voids (marked by arrows in the figure) and a globular surface morphology. The film deposited at 0.6 kW cm^{-2} (Fig. 5.b) also appears columnar with a globular surface morphology but there is a tendency towards denser films with columns packed closely together. At 1.1 kW cm^{-2} the cross-section of the film displays columnar features in the microstructure, but at this higher energy density extensive renucleation has occurred disturbing the growth of the columns causing their fragmentation. The pulsed DCMS film is seen to be columnar with 0.1–0.2 µm wide columns. These findings are in accordance with other studies on both laboratory- and industrial-scale [26,33,34,35] HiPIMS deposition, which have shown that dense and fine-grained films can be deposited due to the intense ion bombardment inherent to HiPIMS deposition.

Fig. 6 shows plan-view SEM micrographs of the HiPIMS films deposited at different peak power densities as well as the pulsed DCMS reference film. For films deposited at 0.4 kW cm^{-2} (Fig. 6.a) and

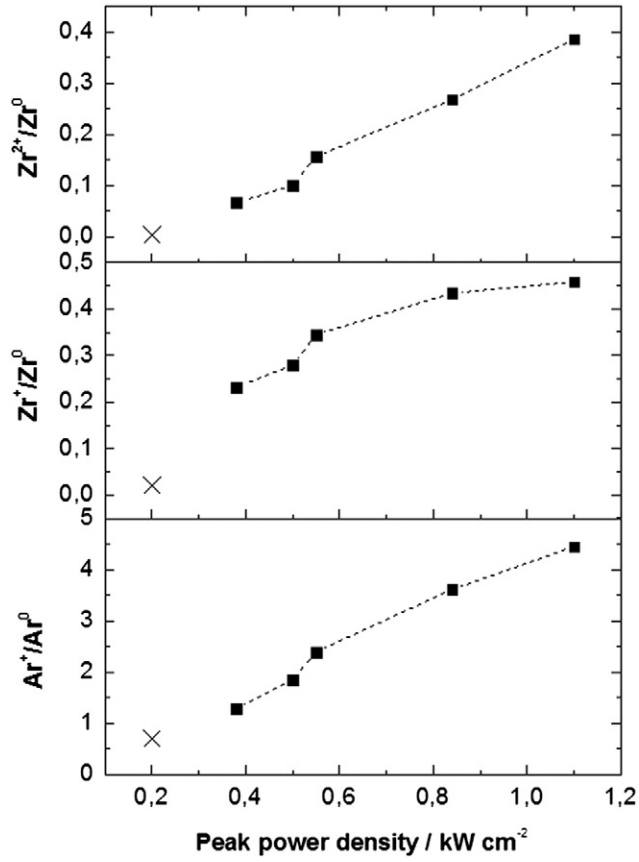

Fig. 4. Ratio of the integrated intensity of the ionized and neutral emission lines of Ar and Zr as a function of peak power. The cross marks the ratio for pulsed DCMS. The intensities for the lines at 763.5 nm (Ar^0), 480.6 nm (Ar^+), 468.7 nm (Zr^0), 262.0 nm (Zr^{2+}) and 256.8 nm (Zr^+) are used.

0.6 kW cm^{-2} (Fig. 6.b) the underlying morphology of the substrate is seen to be reproduced in the coating and there is no apparent difference between the two films. For the DCMS film (Fig. 6.d) the open structure also seen in the cross-section micrograph is observed. The film deposited at 1.1 kW cm^{-2} (Fig. 6.c) has a nodular surface morphology and the reproduction of the features of the substrate is significantly reduced.

The evolution in film morphology observed in Fig. 5 can be related to the degree of ionization of plasma, and the corresponding kinetic energy of the incident species, as seen in Fig. 4. However, it should be noted that bombardment by negative oxygen ions will also affect the resulting film structure; this effect is known from a zirconia-based system [36] and from other oxide systems [37–39]. Likewise, the peak power density setting has been controlled by applying different repetition frequencies, which is also known to influence the film structure in reactive deposition processes [40,41]. The film prepared by pulsed DCMS was deposited under conditions where the ionization of the Ar gas was low and where very few of the sputtered species were ionized. Therefore, only few ionic species bombard the surface of the growing film and increase adatom mobility; any kinetic energy imparted by ion bombardment is due to Ar+ ions accelerated by the substrate bias. In combination with the relatively low deposition temperature (below 300 °C) and substrate bias voltage (−60 V), the adatom mobility was therefore low. The fibrous, faceted structure observed in Figs. 5.d and 6.d is typical for films grown in zone T in the structure zone model (SZM) formalism where a columnar structure forms from an initially random orientated layer due to competitive growth [42]. In the HiPIMS depositions the degree of ionization of the plasma is higher. As a consequence, more ionic gas species bombard the surface of the growing film and thus increase adatom mobility. In addition, the increased metal ion fraction in the sputtered flux has kinetic energy corresponding to the substrate bias (60 eV) and

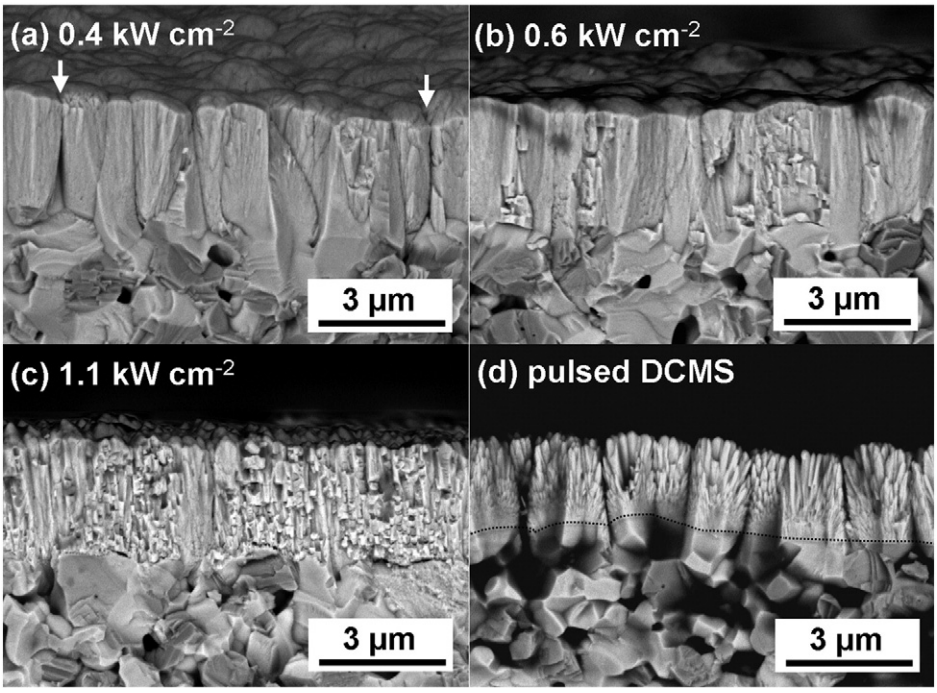

Fig. 5. SEM cross-section micrographs of HiPIMS deposited films grown at peak power densities of (a) 0.4 kW cm^{-2}, (b) 0.6 kW cm^{-2}, (c) 1.1 kW cm^{-2} and (d) pulsed DCMS for comparison. In (a) open column boundaries are marked by arrows. In (d) a dashed line marks the substrate–film interface.

which is the most important contribution to the enhanced adatom mobility. Therefore, the morphology of the film deposited at 0.4 kW cm^{-2} (Figs. 5.a and 6.a) is considerably denser than the film deposited by pulsed DCMS. As the peak power density is increased to 0.6 kW cm^{-2} the degree of ionization of both Ar and metal species gets higher and more doubly ionized metal ions are formed (see Fig. 4). This results in an additional increase in adatom mobility and denser films. As the peak power is further increased so is the degree of ionization and the

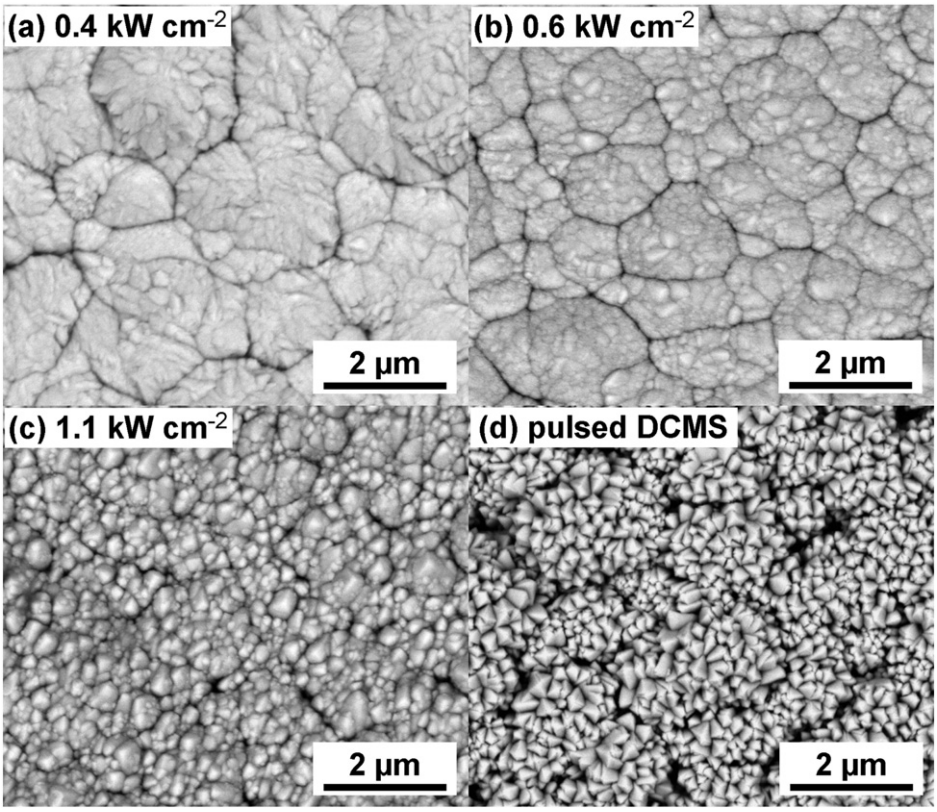

Fig. 6. Plan-view SEM micrographs of HiPIMS deposited films grown at peak power densities of (a) 0.4 kW cm^{-2}, (b) 0.6 kW cm^{-2}, (c) 1.1 kW cm^{-2} and (d) pulsed DCMS for comparison.

number of doubly ionized metal ions as seen in Fig. 4. It is certain that the kinetic energy of the singly ionized ions is increased [43], but the doubly ionized species are of particular interest as they gain twice as much kinetic energy as the singly ionized species when accelerated by the substrate bias voltage. The ion bombardment is so intense that the columnar film growth is disrupted by renucleation (Figs. 5.c and 6.c).

Deposition rates for the different deposition conditions are seen in Table 1. Pulsed DCMS is seen to have a higher deposition rate than HiPIMS as is often observed [20,21], a result of back attraction of metal ions followed by self-sputtering [44] and loss of sputtered material by sideways deposition [45]. This effect is more pronounced for high degrees of ionization resulting from higher peak powers (and thereby lower repetition frequency as the average power is kept constant). This is in agreement with previous reports [34].

3.3. Influence of bias voltage

Besides the ion-to-neutral ratio in the deposition flux, which can be tuned by adjusting the cathode peak power, the kinetic energy of the bombarding ions influences film morphology by influencing adatom mobility and nucleation rates [46]. To investigate this parameter, films were deposited with an applied substrate bias of −60 V, −120 V, and −180 V. In order to maintain an acceptable deposition rate from an industrial point of view and at the same time achieve dense films, the repetition frequency was set to achieve a peak power density of 0.6 kW cm^{-2} and the pressure to ~750 mPa.

Fig. 7 shows plan-view and cross-section SEM micrographs of films deposited at −120 V and −180 V. These are to be compared with the film deposited at −60 V shown in Figs. 5.b and 6.b. As can be seen from the plan-view SEM images (Figs. 6.b and 7.a), the films reproduce the underlying morphology of the substrate and there is no apparent difference in the surface morphology. The cross-sectional SEM micrographs show progress towards denser films. The films deposited at −60 V (Fig. 5.b) and −120 V (Fig. 7.b) appear to have a similar columnar structure but the film deposited at −180 V (Fig. 7.c) has a more uniform and essentially non-columnar structure. The increased density is a consequence of the increased kinetic energy of the bombarding species [37]. Increasing the substrate bias also decreases the deposition rate from 0.42 μm h^{-1} at −60 V to 0.21 μm h^{-1} at −180 V (see Table 1). The decreased deposition rate is likely to be a result of both resputtering and densification of the deposited films as observed in Fig. 5. The structure observed in the film deposited at −180 V appears dense and is thus interesting as a potential electrolyte in SOFC applications.

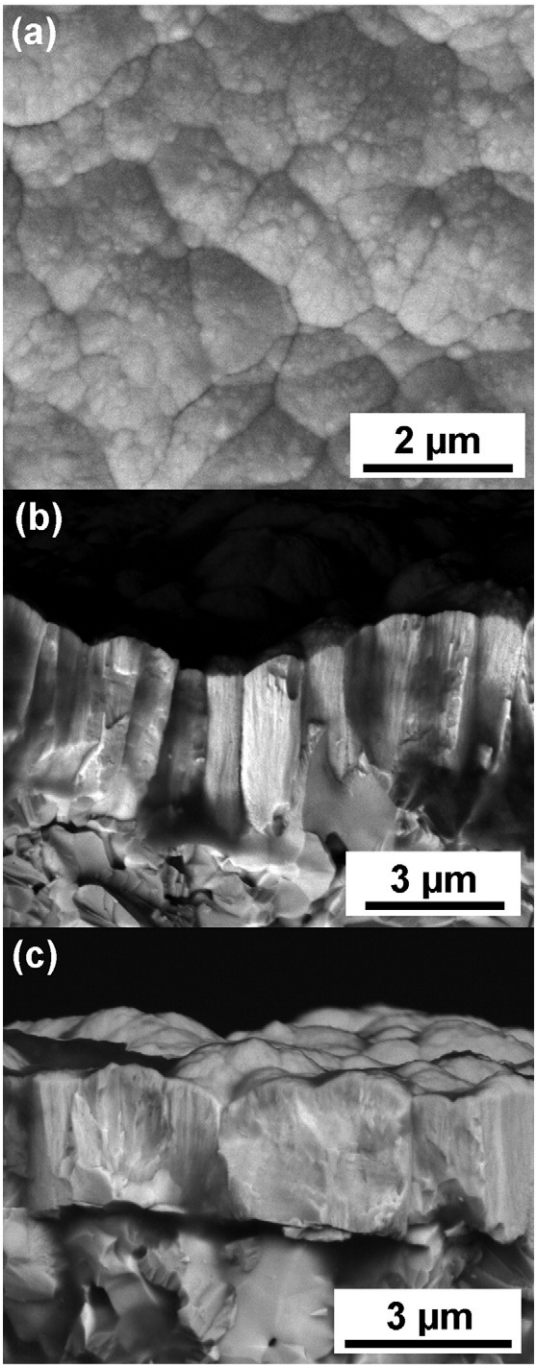

Fig. 7. SEM micrographs of films deposited at bias voltages −180 V (a, c) and −120 V (b). The peak power density was 0.6 kW cm^{-2} and the deposition pressure ~750 mPa.

4. Conclusions

Industrial-scale reactive HiPIMS deposition of YSZ coatings was studied by investigating the effects of deposition pressure, cathode peak power density, and substrate bias voltage on the film morphology and deposition rate. Deposition pressures of ~370 mPa and ~750 mPa were compared and it was found that increasing the pressure to ~750 mPa resulted in a 64% increase in deposition rate and denser films. This was attributed to the presence of more ionic species for sputtering and for bombarding the growing film which increased adatom mobility. As a consequence the subsequent depositions were carried out at ~750 mPa. X-ray diffractograms of film deposited on Si showed all deposited films to be of the desired cubic phase. The films were found to be <220> textured when the bombarding ions had low kinetic energy. The <220> texture resulted from competitive growth but as the ion bombardment became more energetic the texture changed to <200> due to channeling.

Films deposited by pulsed DCMS on polycrystalline NiO–YSZ substrates were columnar and had an open structure and in comparison the HiPIMS deposited films were significantly denser. When varying the cathode peak power density it was found that the degree of ionization of both Ar and sputtered metallic species could be significantly increased. When increasing the peak power density from 0.4 kW cm^{-2} to 0.6 kW cm^{-2} the concentration of open column boundaries seemed to decrease but the films remained columnar. The film densification could be related to the increased flux of ionic species bombarding the growing film and increasing adatom mobility. Increasing the peak power density to 1.1 kW cm^{-2} resulted in a disrupted film growth due to the energetic ion bombardment. The increase in peak power also resulted in a significant drop in deposition rate due to lower repetition frequency and probably also back attraction of ionized sputtered particles as well as sideways deposition. It was found that by combining a peak power density of 0.6 kW cm^{-2} with the application of −180 V substrate bias the columnar structure could essentially be

removed resulting in a uniform structure which may be suitable for industrial SOFC applications.

Acknowledgments

The financial support from Nordforsk ref. no. 9046 (ThinSOFT), Nordic Innovation Centre ref. no. 09046 (Thin-SOFC), and the Swedish Foundation for Strategic Research (Ingvar Carlsson Award 3 and Future Research Leaders 5), is acknowledged. Furthermore, the work has been supported by COST action MP0804.

References

[1] S.J. Litzelman, J.L. Hertz, W. Jung, H.L. Tuller, Fuel Cells 8 (2008) 294.
[2] M.C. Tucker, J. Power Sources 195 (2010) 4570.
[3] L.R. Pederson, P. Singh, X.-D. Zhou, Vacuum 80 (2006) 1066.
[4] D. Beckel, A. Bieberle-Hütter, A. Harvey, A. Infortuna, U.P. Muecke, M. Prestat, J.L.M. Rupp, L.J. Gauckler, J. Power Sources 173 (2007) 325.
[5] N.H. Menzler, F. Tietz, S. Uhlenbruck, H.P. Buchkremer, D. Stöver, J. Mater. Sci. 45 (2010) 3109.
[6] G. Garcia, J. Caro, J. Santiso, J.A. Pardo, A. Figueras, A. Abrutis, Chem. Vap. Depos. 9 (2003) 279.
[7] J.H. Shim, C.-C. Chao, H. Huang, F.B. Prinz, Chem. Mater. 19 (2007) 3850.
[8] T. Van Gestel, D. Sebold, H.P. Buchkremer, D. Stöver, J. Eur. Ceram. Soc. 32 (2012) 9.
[9] H. Hidalgo, E. Reguzina, E. Millon, A.-L. Thomann, J. Mathias, C. Boulmer-Leborgne, T. Sauvage, P. Brault, Surf. Coat. Technol. 205 (2011) 4495.
[10] S. Cho, Y. Kim, J.-H. Kim, A. Manthiram, H. Wang, Electrochim. Acta 56 (2011) 5472.
[11] M. Sillassen, P. Eklund, M. Sridharan, N. Pryds, N. Bonanos, J. Bøttiger, J. Appl. Phys. 105 (2009) 104907.
[12] F. Smeacetto, M. Salvo, L.C. Ajitdoss, S. Perero, T. Moskalewicz, S. Boldrini, L. Doubova, M. Ferraris, Mater. Lett. 64 (2010) 2450.
[13] P. Briois, A. Billard, Surf. Coat. Technol. 201 (2006) 1328.
[14] S. Rey-Mermet, Y. Yan, C. Sandu, G. Deng, P. Muralt, Thin Solid Films 518 (2009) 4743.
[15] S. Sønderby, A.J. Nielsen, B.H. Christensen, K.P. Almtoft, J. Lu, J. Jensen, L.P. Nielsen, P. Eklund, Surf. Coat. Technol. 206 (2012) 4126.
[16] R. Nédélec, S. Uhlenbruck, D. Sebold, V.A.C. Haanappel, H.-P. Buchkremer, D. Stöver, J. Power Sources 205 (2012) 157.
[17] H.G. Scott, J. Mater. Sci. 10 (1975) 1527.
[18] T. Klemensø, J. Nielsen, P. Blennow, Å.H. Persson, T. Stegk, B.H. Christensen, S. Sønderby, J. Power Sources 196 (2011) 9459.
[19] V. Kouznetsov, K. Macák, J.M. Schneider, U. Helmersson, I. Petrov, Surf. Coat. Technol. 122 (1999) 290.
[20] U. Helmersson, M. Lattemann, J. Bohlmark, A.P. Ehiasarian, Thin Solid Films 513 (2006) 1.
[21] K. Sarakinos, J. Alami, S. Konstantinidis, Surf. Coat. Technol. 204 (2010) 1661.
[22] K. Macák, V. Kouznetsov, J. Schneider, U. Helmersson, I. Petrov, J. Vac. Sci. Technol. A 18 (2000) 1533.
[23] J. Bohlmark, M. Lattemann, J. Gudmundsson, A. Ehiasarian, Y. Arandagonzalvo, N. Brenning, U. Helmersson, Thin Solid Films 515 (2006) 1522.
[24] H. Hidalgo, A.-L. Thomann, T. Lecas, J. Vulliet, K. Wittmann-Teneze, D. Damiani, E. Millon, P. Brault, Fuel Cells 13 (2013) 279.
[25] P. Coddet, M.-C. Pera, A. Billard, Fuel Cells 11 (2011) 158.
[26] J. Alami, K. Sarakinos, F. Uslu, M. Wuttig, J. Phys. D. Appl. Phys. 42 (2009) 015304.
[27] S. Sønderby, A. Aijaz, U. Helmersson, K. Sarakinos, P. Eklund, Surf. Coat. Technol. 240 (2014) 1.
[28] W.D. Sproul, D.J. Christie, D.C. Carter, Thin Solid Films 491 (2005) 1.
[29] S. Kadlec, C. Quaeyhaegens, G. Knuyt, L.M. Stals, Surf. Coat. Technol. 89 (1997) 177.
[30] S. Mahieu, P. Ghekiere, G. De Winter, D. Depla, R. De Gryse, O.I. Lebedev, G. Van Tendeloo, Thin Solid Films 484 (2005) 18.
[31] A.N. Reed, M.A. Lange, C. Muratore, J.E. Bultman, J.G. Jones, A.A. Voevodin, Surf. Coat. Technol. 206 (2012) 3795.
[32] S.M. Rossnagel, J.J. Cuomo, Thin Solid Films 171 (1989) 143.
[33] G. Greczynski, J. Lu, J. Jensen, S. Bolz, W. Kölker, C. Schiffers, O. Lemmer, J.E. Greene, L. Hultman, Surf. Coat. Technol. 257 (2014) 15.
[34] N. Bagcivan, K. Bobzin, A. Ludwig, D. Grochla, R.H. Brugnara, Thin Solid Films 572 (2014) 153.
[35] E. Hovsepian, A.P. Ehiasarian, I. Petrov, Surf. Coat. Technol. 257 (2014) 38.
[36] D. Severin, Kostas Sarakinos, O. Kappertz, A. Pflug and M. Wuttig, J. Appl. Phys. 103 (2008) 083306.
[37] O. Kappertz, R. Drese, J.M. Ngaruiya, M. Wuttig, Thin Solid Films 484 (2005) 64.
[38] S. Mahieu, D. Depla, Appl. Phys. Lett. 90 (2007) 121117.
[39] S. Mraz, J.M. Schneider, Appl. Phys. Lett. 89 (2006) 51502.
[40] R. Ganesan, B.J. Murdoch, B. Treverrow, A.E. Ross, I.S. Falconer, A. Kondyurin, D.G. McCulloch, J.G. Partridge, D.R. McKenzie, M.M.M. Bilek, Plasma Sources Sci. Technol. 24 (2015) 035015.
[41] T. Kubart, J. Andersson, IOP Conf. Ser.: Mater. Sci. Eng. 39 (2012) 012008.
[42] S. Mahieu, P. Ghekiere, D. Depla, R. De Gryse, Thin Solid Films 515 (2006) 1229.
[43] M. Aiempanakit, U. Helmersson, A. Aijaz, P. Larsson, R. Magnusson, J. Jensen, T. Kubart, Surf. Coat. Technol. 205 (2011) 4828.
[44] D.J. Christie, J. Vac. Sci. Technol. A 23 (2005) 330.
[45] D. Lundin, P. Larsson, E. Wallin, M. Lattemann, N. Brenning, U. Helmersson, Plasma Sources Sci. Technol. 17 (2008) 035021.
[46] I. Petrov, P.B. Barna, L. Hultman, J.E. Greene, J. Vac. Sci. Technol. A 21 (2003) S117.